SECURITY CLASSIFICATION OF THIS PAGE

(2)

REPORT DOCUMENTATION PAGE

AD-A213 511

LE

1b RESTRICTIVE MARKINGS: None

3. DISTRIBUTION / AVAILABILITY OF REPORT: Approved for public release and sale. Distribution unlimited.

4. PERFORMING ORGANIZATION REPORT NUMBER(S): Technical Report # 12

5. MONITORING ORGANIZATION REPORT NUMBER(S):

6a. NAME OF PERFORMING ORGANIZATION: California Institute of Technology

6b. OFFICE SYMBOL (If applicable):

7a. NAME OF MONITORING ORGANIZATION: Office of Naval Research

6c. ADDRESS (City, State, and ZIP Code): Noyes Laboratory of Chemical Physics, California Institute of Technology, Pasadena, CA 91125

7b. ADDRESS (City, State, and ZIP Code): Chemistry Program, Arlington, Virginia 22217

8a. NAME OF FUNDING / SPONSORING ORGANIZATION: Office of Naval Research

8b. OFFICE SYMBOL (If applicable):

9. PROCUREMENT INSTRUMENT IDENTIFICATION NUMBER: N00014-89-J-1278

8c. ADDRESS (City, State, and ZIP Code): Chemistry Program, 800 N. Quincy Street, Arlington, Virginia 22217

10. SOURCE OF FUNDING NUMBERS

PROGRAM ELEMENT NO	PROJECT NO.	TASK NO	WORK UNIT ACCESSION NO
		4133004 ---02	

11. TITLE (Include Security Classification): Dynamics of Electron Transfer for a Non-superexchange Coherent Mechanism. II. Numerical Calculations

12 PERSONAL AUTHOR(S): R. Almeida and R. A. Marcus

13a. TYPE OF REPORT	13b. TIME COVERED	14. DATE OF REPORT (Year, Month, Day)	15. PAGE COUNT
Technical Report	FROM 8/1/88 TO 10/13/89	89, 10, 13	38

16. SUPPLEMENTARY NOTATION

17. COSATI CODES			18. SUBJECT TERMS (Continue on reverse if necessary and identify by block number)
FIELD	GROUP	SUB-GROUP	

19. ABSTRACT (Continue on reverse if necessary and identify by block number)

The expressions ~~in Part I~~ are used to treat the dynamics of electron transfer in the donor acceptor system D*BA, via a molecular bridge B. Using a Fast Fourier Transform method results are obtained for the maximum "population" of B^- and for other properties for this coherent but nonsuperexchange model. Several approximate ideas on rate populations and energy distributions are tested suing various values for the numerical parameters.

20 DISTRIBUTION / AVAILABILITY OF ABSTRACT: ☒ UNCLASSIFIED/UNLIMITED ☐ SAME AS RPT ☐ DTIC USERS

21 ABSTRACT SECURITY CLASSIFICATION: Unclassified

22a NAME OF RESPONSIBLE INDIVIDUAL	22b TELEPHONE (Include Area Code)	22c OFFICE SYMBOL
R. A. Marcus	818 356-6566	MC 127-72

DD FORM 1473, 84 MAR — 83 APR edition may be used until exhausted. All other editions are obsolete.

SECURITY CLASSIFICATION OF THIS PAGE

Dynamics of Electron Transfer for a Non-superexchange Coherent Mechanism. II. Numerical Calculations

R. Almeida† and R. A. Marcus

*Noyes Laboratory of Chemical Physics**

California Institute of Technology

Pasadena, California 91125

Abstract

The expressions in Part I are used to treat the dynamics of electron transfer in the donor acceptor system D*BA, via a molecular bridge B. Using a Fast Fourier Transform method results are obtained for the maximum "population" of B^- and for other properties for this coherent but nonsuperexchange model. Several approximate ideas on rate populations and energy distributions are tested using various values for the numerical parameters.

† Present Address: Departamento de Quimica, Facultad de Ciencias, Universidad de Los Andes, Merida, edo. Merida 5101, Venezuela

* Contribution No. 8001

I. Introduction

In Part I we explored the dynamics of electron transfer from some donor D* to an acceptor A via a molecular bridge B, using one form of a coherent mechanism.[1] A system was considered such that the relevant orbital of B was readily accessible energetically, so that a superexchange mechanism was not involved, but such that B and A were so strongly coupled electronically that a conventional (incoherent) two-step electron transfer, $D^* \rightarrow B^-$, $B^- \rightarrow A$ involving a chemical intermediate B^- was also not appropriate. In the present article we describe some numerical applications of the formalism outlined in Part I. Synthesis of suitable D*BA systems may permit the observation of this type of mechanism.

In the formalism given in Part I, the nuclear motion accompanying the electron transfer in D*BA was approximated with three collective vibrational coordinates, there being three reactive centers, D*, B, and A. Using equal vibration frequencies to simplify the problem and to extract some of the features, the three-coordinate problem for the electronic-nuclear motion was reduced to a two-coordinate one by a suitable rotation of the coordinate axes. A nonadiabatic mechanism was then used for the initial loss of the electron from D*. The ensuing nuclear motion on the BA potential energy surface was then separable into two one-coordinate motions. Some numerical results based on this formalism are given in the present article to illustrate some of the consequences of the mechanism, particularly for the transient amount of B^-.

We first consider numerically in Section II a simplified treatment, one which contains only one collective coordinate instead of three and which serves to test several features. In particular, results for the decay of D* are explored to see if they are well-represented by a single exponential decay (Section III). The numerical rate constant obtained there is also compared with that found from various Golden rule and semiclassical estimates. In Section III results for this one-coordinate system are

also given for the maximum population of $B^-(t)$, determined by projecting the electronic wavefunction onto a basis set wavefunction describing the D^+B^-A electronic configuration. The question of whether this $B^-(t)$ *appears* to follow, roughly, the kinetics of a two-step electron transfer mechanism, $D^*BA \rightarrow D^+B^-A \rightarrow D^+BA^-$, with successive rate constants k_1 and k_2, but with an abnormally high apparent value for k_2, is explored in Section II. In Section III, results for the three-collective coordinate system are given, and correlations drawn between "B^-_{max}" for various molecular parameters and an effective " elapsed time" in the D^+B^-A configuration.

II. One-coordinate Test Calculation of Several Properties

(*i*) *Formalism*

As in Part I we introduce electronic wavefunctions to describe the three electronic configurations D^*BA ($i=1$), D^+B^-A ($i=2$) and D^+BA^- ($i=3$). In a standard fashion the Schrödinger equation is again converted then into a set of three coupled equations for the nuclear wavefunctions ϕ_i in each electronic state, namely eq. (2.4) of Part I. However, even at the outset there is now only one nuclear coordinate z. Equation (2.4) of Part I can be written for this case in dimensionless quantities as

$$-\tfrac{1}{2}\frac{\partial^2}{\partial z^2}\Phi_i + \sum_{j=1}^{3} H_{ij}\Phi_j = i\frac{\partial \Phi_i}{\partial t} \quad , \tag{2.1}$$

where the H_{ij} represent various electronic matrix elements. As before, $H_{13} \simeq 0$ and H_{12} and H_{23} are treated as constants. The diagonal quantities H_{ii} represent diabatic potential energy curves for the three electronic configurations. In the usual vibrational harmonic approximation, they are

$$\left.\begin{aligned} H_{11} &= \tfrac{1}{2}z^2 \\ H_{22} &= \tfrac{1}{2}(z-a)^2 + \Delta E_{12} \\ H_{33} &= \tfrac{1}{2}(z-b)^2 + \Delta E_{13} \end{aligned}\right\} \qquad (2.2)$$

a and b being equilibrium nuclear displacements for the electronic configurations 2 and 3 relative to that for 1. When the a in eq. (2.2) is chosen so that $a^2 = a_1^2 + a_2^2$, where the a_i's are defined in Part I, the present reorganizational parameter λ_{12} for the $\Psi_1 \rightarrow \Psi_2$ step, namely $\frac{1}{2}a^2$, is the same as that $(\frac{1}{2}a_1^2 + \frac{1}{2}a_2^2)$ in the three-coordinate problem. Similarly, when one sets $b^2 = a_1^2 + a_3^2$, λ_{13} is also the same in the one- and three-coordinate cases. (However, the λ_{23}'s differ.) The H_{ij}'s in (1.1) - (1.2) are, as in Part I, the actual matrix elements divided by $\hbar\omega$, where $\omega/2\pi$ is the vibrational frequency.

In a real system, dissipation of the energy after (and during) the $\Psi_1 \rightarrow \Psi_2 \rightarrow \Psi_3$ transition occurs by redistribution of that energy among the numerous degrees of freedom. To avoid spurious oscillations of the wave packet in the simple model described by eqs. (2.1) - (2.2), after the system has reached the $z \simeq b$ region, the H_{33} in eq. (2.2) is used only for $z < b$, while for $b \leq z \leq L$ the $(z-b)^2$ term is set here equal to its value at $z = b$ and an absorbing boundary is introduced at a boundary,[2] $z = L$, $L > b$. Equation (2.1) was then integrated numerically using a Fast Fourier Transform routine.[3,4] The latter method is briefly summarized in Appendix A.

(ii) Calculation of Rate Constant k_r and Various Approximations

From a semilog plot of the population in state Ψ_1 vs. time, $\int|\phi_1(z, t)|^2 dz$, determined from this FFT solution, a rate constant was calculated. The decay was typically essentially single-exponential, a plot being given in Fig. 1. (Conditions for an alternative damped oscillatory behavior, as in Fig. 3, are given later.) These rate

constants are compared later in Section III with values obtained from several approximate expressions that are summarized in Appendix B.

In each of these latter approximations a Golden Rule expression[5] was used. Written here in terms of one coordinate, the rate constant k_r for reaction from a specific vibrational state m is

$$k_r = 2\pi\omega\,|H_{12}|^2 \sum_{m'} |\langle \phi_m(z)\,|\,\phi_{m'}^{(2)}(z)\rangle|^2\,\delta(E_m - E_{m'}) \quad . \tag{2.3}$$

where $\phi_m(z)$ is the vibrational wavefunction appropriate to $H_{11}(z)$, treated as a harmonic oscillator potential, as in eq. (2.2), and the $\phi_{m'}^{(2)}$ in one approximation denotes a nuclear wavefunction appropriate to $H_{22}(z)$. For comparison, in a different approximation it denotes the eigenfunction ϕ_A appropriate to the lower adiabatic surface $E_-(z)$ arising from the (ψ_2, ψ_3) pair (eq. (2.4) below). The corresponding values of k_r are denoted later in Tables I and II by k_{HO} and k_A, respectively. This k_{HO} is, thereby, the microcanonical version of the usually calculated Golden Rule rate constant in the literature. In an added approximation in each case the final state eigenfunction $\phi_{m'}^{(2)}$ is replaced by its semiclassical stationary phase counterpart. The resulting Franck-Condon matrix element $\langle \phi_m(z)|\phi_{m'}^{(2)}(z)\rangle$ in eq. (2.3) is given by eqs. (B4)-(B8), in both these diabatic and adiabatic choices for $\phi_{m'}^{(2)}$, and the corresponding k_r's are denoted in Tables I and II by k_{HO}^{sc} and k_A^{sc}, respectively. The adiabatic potential curve $E_-(z)$ referred to above is given by

$$E_-(z) = \tfrac{1}{2}\{[H_{22}(z) + H_{33}(z)] - \{[H_{22}(z) - H_{33}(z)]^2 + 4H_{23}^2\}^{\frac{1}{2}}\} \tag{2.4}$$

When the initial vibrational state m is 0 in Tables I and II, the energy of the initial vibrational state was close to ΔV_1, the potential energy at the crossing point of $H_{11}(z)$ and $H_{22}(z)$ potential energy curves (cf. ref. 6, eq. (2)),

$$\Delta V_1 = (\lambda_{12}/4)\,(1+\Delta E_{12}/\lambda_{12})^2 \quad . \tag{2.5}$$

For this case, namely for all $m=0$ cases in Tables I and II, a uniform approximation (Airy function), given by eq. (B7), was used for the semiclassical matrix element.

(*iii*) *Effective rate constant k_2 for the disappearance of* $B^-(t)$

Both for the one- and the three-coordinate calculations it is useful to know whether the coherent dynamics for the "$B^-(t)$", obtained numerically, can be fitted by an apparent two-step kinetic equation, in which the effective rate constant k_2 of the second step is much larger than the theoretical adiabatic maximum for k_2 in a two-step (incoherent) process, namely $\omega/2\pi$. A method of defining $B^-(t)$, by projecting the time-dependent wavefunction onto the diabatic state ψ_2 and integrating over the nuclear coordinates, was used in Part I (eq. (4.8)). The corresponding equation for the one-coordinate case is

$$B^-(t) = \int dz\,|\langle \psi(z,t)|\,\psi_2\rangle|^2 = \int dz\,|\phi_2(z,t)|^2 \tag{2.6}$$

In order to interpret the results on k_2 an estimate is needed for the region approximately corresponding to "B^-" during the motion along the z-axis. As in Part I we take it to be, roughly, the distance between the intersection of the $H_{11}(z)$ and $H_{22}(z)$ curves, which occurs at $z_{12}^{\ddagger}$, and the intersection of the $H_{22}(z)$ and $H_{33}(z)$ curves, which occurs at $z_{23}^{\ddagger}$. Using the arguments which led, in Part I, to eqs. (5.5) and (5.6) there for $z_{23}^{\ddagger}$, and using an identical argument for $z_{12}^{\ddagger}$, but with ΔE_{12} replacing ΔE_{23} and λ_{12} replacing λ_{23}, we obtain

$$z_{23}^{\ddagger} - z_{12}^{\ddagger} = (\lambda_{23}+\Delta E_{23})(2\lambda_{23})^{-\frac{1}{2}} + (\lambda_{12}-\Delta E_{12})(2\lambda_{12})^{-\frac{1}{2}} \tag{2.7}$$

Again, as in Part I, if the local velocity in this region is denoted by v_z, we have $v_z=[2\{E_z-H_{22}(z)+H_{22}(z_2^\circ)\}]^{\frac{1}{2}}$, or if the $E_-(z)$ curve had been used instead of the $H_{22}(z)$ one, $v_z=[2\{E_z-\mathrm{E}_-(z)+E_-(z_2^0)\}]^{\frac{1}{2}}$, both as in Part I, where E_z is the initial energy. A rough approximation to k_2 is given by

$$k_2 \sim \bar{v}_z/|z_{23}^{\ddagger}-z_{12}^{\ddagger}| \qquad \text{(when } w_{23}\sim 1)\ , \tag{2.8}$$

where $\bar{v}_z$ is some mean z-velocity in the above z-interval, as in eq. (5.9) of Part I, and w_{23} is the probability of a 2→3 transition when the system crosses the "intersection region" at $z=z_{23}^{\ddagger}$.

(iv) The rate constant k_r for the three-coordinate calculations

The Golden Rule approximation was used for k_r for the three-coordinate system. The parameters were chosen to yield some fixed value of k_r for an initial vibrational state $m=0$, so as to explore the effect of several other parameters when the rate constant for *formation* of the population "$\mathrm{B}^-(t)$" was held fixed. The low temperature standard form of the rate constant was used, since it corresponds to reaction from $m=0$ (cf. ref. 6, eq. (71)):

$$k_r = 2\pi\omega|H_{12}|^2\, e^{-\lambda_{12}}\lambda_{12}^{p}/\Gamma(p+1) \quad (0^\circ\mathrm{K})\ , \tag{2.9}$$

where $p=-\Delta E_{12}$.

(v) The intermediate population "$\mathrm{B}^-(t)$" for the three-coordinate calculation

The dynamics of the population $\mathrm{B}^-(t)$ of the intermediate B^- was computed for two different potential energy surfaces for the (2, 3) pair of states. For the first of these surfaces, calculations of $\mathrm{B}^-(t)$ were made using the coupled diabatic states, the analog of the present eq. (2.1), described in Part I and in the second, for comparison, a

purely adiabatic (2, 3) surface $E_-(y, z)$ there was used, the analog of the present eq. (2.4). The time-dependent Schrödinger equation was also described in Part I. The numerical treatment was made for the one-coordinate numerical integration over the z-motion (eq. (4.7) of Part I), which followed from an analytical separation of the x and y motion there from that of z. Details of the numerical (FFT) method are given in Appendix A.

The three-coordinate analog of eq. (2.7) for the region $z_{23}^{\ddagger} - z_{12}^{\ddagger}$ occupied by "B^-" was obtained in Part I:

$$z_{23}^{\ddagger} - z_{12}^{\ddagger} = [(\Delta E_{23} + \lambda_{23}) + (\Delta E_{12} - \lambda_{12})(\lambda_2/\lambda_{12})] \ /(2\lambda_{23})^{\frac{1}{2}} \quad , \tag{2.10}$$

and eq. (2.8) is used for k_2.

III. Results

(*i*) *One-coordinate k_r's*

The results for the FFT-calculated time-evolution of the population of the initial electronic configuration 1 typically followed a first-order kinetics plot after a brief transient period, as in Fig. 1, and so was describable by a first-order rate constant. These one-coordinate calculations were made for Tables I and II using values of the parameters specified there in the footnotes.

The rate constants obtained from the numerical (FFT) solution for k_r are denoted in Tables I and II by k_1 and are compared there with those obtained using the various approximations described earlier in section II(*ii*) and in Appendix B. A comparison with the semiclassical results is helpful in providing some insight on the dependence of k_r on the initial vibrational state and on the dependence of the quantum-calculated populations $B^-(t)$ on various parameters.

To represent the results of the many $B^-(t)$ vs. t curves it is useful to see whether they are describable phenomenologically, for the range of parameters chosen, by an apparent two-step sequence,[1] with rate constants k_1 and k_2, where k_2 is now an effective rate constant, an adjustable parameter. This possibility was explored here for a number of cases, an example of such a fit being given in Fig. 2. The fitted k_2 there is 24 ps^{-1}, which is eight times the maximum adiabatic value of (at $\hbar\omega = 100$ cm^{-1}) 3 ps^{-1}. Other results for fitted k_2's are given in Table III. Also given there are the sizes of the region $z_{23}^{\ddagger} - z_{12}^{\ddagger}$, "occupied" by B^-. It is easy to find molecular parameters for which such a two-step phenomenology is inappropriate, for example, when w_{23} is deliberately made very small,[7] an example is being given in Fig. 3. Here, the decay of $D^*(t)$ is strongly oscillatory, in contrast with the behavior in Fig. 2, where the decay is largely monotonic. (The absence of a dissipative term in the D^+B^- A stage of the model permits the oscillations to occur.)

(*ii*) *Three-coordinate* k_r, B^-_{max} and $\langle n' \rangle$

The population of $B^-(t)$ was studied numerically here for the case where the k_r calculated from the Golden Rule eq. (2.9) for $m=0$ was 0.92 ps^{-1}. The parameters used are given in Table IV. A small value of λ_2 corresponds to a bridge with negligible reorganization energy. Two sets of values for the ratio H_{23}/H_{12} are used, namely 10 and 6. In each calculation the maximum of the intermediate population is given in Table IV. This maximum B^- population is denoted there by B_{max}^-, when all matrix elements, $H_{22}(z)$, $H_{33}(z)$ and $H_{23}(z)$ are used in the propagation (eq. (A11) for H_z) and by $B_{ad,max}^-$ when, for comparison, only H_z^{ad} is used (eq. (A12)). Plots of B_{max}^- and of $B_{ad,max}^-$ for $H_{23}/H_{12} = 6$ and 10 are given in Figs. 4-7.

Two plots of $B^-(t)$ vs. t are given in Figs. 8 and 9, with a fit (adjusting only k_2) to the two-step sequential formalism. Fig. 8 corresponds to the ninth row of Table IV ($H_{23}/H_{12} = 10$) and the fit yields a k_2 of 22 ps^{-1}. Fig. 9 corresponds to the fourth row

from the bottom (H_{23}/H_{12} = 10) and the fitted k_2 is 12 ps^{-1}. In a third result, corresponding to the same row but with H_{23}/H_{12} = 6, the fitted k_2 was only 4.5 ps^{-1}. This last value is seen to be smaller than the corresponding k_2 at H_{23}/H_{12} = 10, presumably because of some reflection of the wave packet at the crossing of the $H_{22}(z)$ and $H_{33}(z)$ potential energy curves. All of these k_2's are higher than the maximum adiabatic value for k_2 of 3 ps^{-1} (at $\hbar\omega = 100\ cm^{-1}$).

In two of the above cases the distribution of the y-vibrational states in the wave packet was analyzed. In the case of the ninth row in Table IV, with H_{23}/H_{12} = 6, the population distribution peaked at n' = 4, with an average value $\langle n' \rangle$ of 3.9. In the case of the fourth row from the bottom in Table IV, with H_{23}/H_{12} = 10, the population peaked between n' = 4 and 5, with an average value $\langle n' \rangle$ of 4.8. The values of $\langle n' \rangle$ predicted from the classical expressions, eq. (5.1) of Part I, if the system after the 1→2 transition moved on the H_{22} surface, is 3.5 and 3.4, respectively, which are substantially less than the observed $\langle n' \rangle$'s of 3.9 and 4.8, respectively. However, if the system near (y^0_2, z^0_2) is better described as moving on the E_- surface rather than the H_{22} as a result of the 1→(2,3) transition, use of eq. (5.3) of Part I shows that the additional energy shared among the (y,z) motion is, in the above units, about 0.8 and 1.7, respectively. If, as in the diabatic case for the parameters chosen the large proportion of the excess goes into E_y, the predicted $\langle n' \rangle$ could then be as large as 4.3 and 5.1. Thus, the diabatic (3.5 and 3.4) and adiabatic (4.3 and 5.1) values for n') bracket, in each case, the observed $\langle n' \rangle$'s, 3.9 and 4.8, respectively. It seems clear that the system after the 1→2 transition has, due to the (2,3) electronic coupling, sensed the presence of the $E_-(z)$ adiabatic surface at z_2^0.

IV. Discussion

(i) One-coordinate k_r's

From the results in Tables I and II there is seen to be reasonable agreement between the one-coordinate numerically-calculated (FFT) reaction rates and those inferred from the various approximations. The use of adiabatic final state wavefunction, leading to the adiabatic rate constants k_A and their semiclassical counterparts k_A^{sc}, is seen to lead to a slightly better agreement, on the average, with the numerical values, k_1, than does the harmonic-calculated rate constant k_{HO} (or k_{HO}^{sc}), particularly for the smaller k_r's. Nevertheless, for our other purposes we have used the k_{HO} in the subsequent calculations for the three-coordinate system, since the k_{HO} expression, eq. (2.9), is particularly simple, and since k_{HO} is rather close to k_A, particularly for $m = 0$, for the parameters chosen. Use of k_A might also have entailed consistency questions regarding the effective electronic matrix element to be used instead of H_{12} in the Golden Rule expression, eq. (2.3). Plots of $k_r(T)$ (not shown), which tend to average over the differences in the various calculations for different m's, were all very similar for the parameters examined.

The substantial decrease in the numerically-calculated k_1's on going from $m = 0$ to $m = 1$ in Tables I and II, and the various oscillations of k_1 with m there, can be seen to be due, in semiclassical terms, mainly to variations in the phase angle in the matrix element for the overlap of the vibrational wavefunctions, for example in the sine term in eq. (B4). When the results are canonically-averaged to yield a temperature-dependent rate constant, there is an averaging over these oscillations and, in fact, the results for $k_r(T)$ were usually close to those which are obtained when the $\sin^2$ term for each $m \geq 1$ term was replaced by an average value, 1/2.

Plots of $k_r(T)$ vs. the temperature T typically had a negative temperature dependence when ΔV_1, given by eq. (2.5), was smaller than the zero-point energy, $\hbar\omega/2$ (50 cm^{-1} in the present case), i.e., whenever the ΔV_1 in dimensionless units was below 0.5. For all of the results in Table IV ΔV_1 is in the neighborhood of 0.2.

(ii) Population of B^-

(a) Maximum Value, B^-_{max}

It is useful to compare the results for the maximum population of B^-, B^-_{max}, given in Table IV and Figs. 6 and 7, with those which would be calculated from an incoherent mechanism, namely a mechanism in which the electron hops from D* to B and then to A. If the rate constants for the $D^* \rightarrow B^-$ and $B^- \rightarrow A^-$ are, as denoted earlier, k_1 and k_2, the maximum population of B^- by this mechanism during the reaction, B^-_{max}, is given by[12]

$$B^-_{max} = \left(\frac{k_1}{k_2}\right)^{\frac{k_2}{k_2 - k_1}} \qquad (4.1)$$

If we use the value $0.92\ 10^{12}\ s^{-1}$ for k_1, and use the maximum adiabatic value $\omega/2\pi$ for k_2, which for the given frequency, is $3\ 10^{12}\ s^{-1}$ ($100\ cm^{-1}$), then B^-_{max} is estimated from eq. (4.1) to be about 18%. Examination of the results for B^-_{max} in Table IV and Figs. 4 and 5 shows that they are appreciably less than this value, reflecting the coherency of the overall $D^* \rightarrow A^-$ electron transfer in the present model. Thus, if eq. (4.1) were used to fit the observed B^-_{max}, an *effective* k_2 much larger than this maximum adiabatic value would occur for the present mechanism. Indeed, the results in Table III illustrate this point, the effective k_2 in the examples cited being a factor of eight larger than the maximum adiabatic value.

Examination of the results in Table IV and Figs. 4-7 reveals a number of additional features, particularly in the comparison of B_{max}^- and $B_{ad,max}^-$. Differences between the two reflect a reflection of the wavepacket at the (2, 3) intersection in the B_{max}^- case. The differences in Table IV and Figs. 5 and 7, for the parameters used, are relatively small (columns $B_{ad,max}^{-(c)}$ and $B_{max}^{-(c)}$) and are larger at a somewhat smaller H_{23} (columns $B_{ad,max}^{-(b)}$ and $B_{max}^{-(b)}$ and Figs. 4 and 6). Further, there is seen

in Fig. 4 to be a correlation between $z_{23}^{\ddagger} - z_{12}^{\ddagger}$ and the value of B_{max}^{-}, for various series of the λ's. A correlation also exists in Fig. 5. The scatter in that figure at small $z_{23}^{\ddagger} - z_{13}^{\ddagger}$ may be due to complexities in the overlapping of the two surface crossings when H_{23} is large, but it was not explored. In plots of $B_{ad,max}^{-}$ in Figs. 6 and 7, these complexities are absent (only one surface crossing), and there is seen to be less scatter.

It is useful to consider a few examples for the rough estimate of $B_{ad,max}^{-}$ based on eqs. (2.7), (2.8) and (4.1) and to compare the estimate with values in Table IV. Two examples are given, both where the *y*-coordinate acquires most of the excess energy $-\Delta E_{12}$ during the motion in H_{22} after the (1→2,3) transition. In this case the systems have an excess *z*-mode energy E_z of about $\hbar\omega/2$ (0.5 in dimensionless units) in the vicinity of z_2^{o}. They have somewhat less than this amount in the vicinity of $z_{12}^{\ddagger}$ and somewhat more in the vicinity of $z_{23}^{\ddagger}$. The velocity v_z in dimensionless units is 1 (since $\frac{1}{2}v_z^2 = \frac{1}{2}$). Averaging two results in Table IV of $B_{ad,max}^{-(c)}$ of 4.1% and 4 3% for the case where $z_{23}^{\ddagger} - z_{12}^{\ddagger}$ equals 0.48 and 0.68, in dimensionless units, respectively, we see that k_2 ($= 1/\tau_2$) is about 1.8 in dimensionless units. Conversion to ps by multiplying by ω yields 34 ps^{-1} for k_2. Equation (4.1) then yields 2.3% for $B_{ad,max}^{-}$, compared with the actual value of 4.2%. Similarly, when $B_{ad,max}^{-}$ is averaged over the last five values in Table IV, it is about 6.3%, $z_{23}^{\ddagger} - z_{12}^{\ddagger}$ is about 0.8, and so $k_2 \simeq$ 1/0.8, i.e. 1.25 in dimensionless units. This value corresponds to a k_2 of 24 ps^{-1} and thereby to a $B^{-}_{ad,max}$ of 3.4% according to eq. (4.1), again roughly a factor of two smaller than the observed value of 6.3%. These values of k_2 may be compared with those of about 25 ps^{-1} estimated by fitting the data of one-coordinate calculations (Table III) to a two-step type kinetic expression.

As a footnote we consider the question of an elementary step in the bacterial photosynthetic reaction center. In this case it has been suggested[8] in the interpretation of some low temperature data on both *Rps viridis* and *Rb. sphaeroides*

that an electron transfer from an electronically-excited bacteriochlorophyll dimer $BChl_2$ to a pheophytin BPh via a chlorophyll monomer BChl, the estimated maximum population of $BChl^-$ could not exceed 2%. The value for the initial rate constant k_1 for forming $BChl^-$ was close to that employed in this paper. Examination of the B_{max}^- in Figs. 4 and 5 shows no results close to this value. (Results with $\lambda_2 = 0.1$ are intended only to simulate a rigid bridge. For BChl a substantially larger λ_2 is expected.) However, perhaps the 2% estimate in ref. 8 is only at rough one. Recently, new and dramatic results[9] have been obtained for *Rb. sphaeroides* at room temperature, showing a substantial value for B^-_{max} and with $k_2/k_1 \simeq 4$. In the latter work an improved signal to noise ratio and improved time-resolution was used, together with observations of the polarization of the absorption. Studies in that laboratory at low temperatures are planned to compare with those obtained[8] earlier. At present, it should be added, none of these results, old and new, is universally accepted, and further published works will be needed before the issue of mechanism is settled.

Acknowledgment

Acknowledgment is made to the Office of Naval Research and to the Donors of the Petroleum Research Fund administered by the Americal Chemical Society for the support of this research. One of us (R. A.) would like to express his appreciation to Professor Horia Metiu for his hospitality and support while he was at the University of California at Santa Barbara.

Appendix A. The Fast Fourier Transform Method

In the calculations made in this paper, a one-dimensional vibrational wave function was propagated using a Fast Fourier Transform (FFT) method.[3b] For completeness it is reviewed briefly here. In the method an operator $\exp(-itH_z)$ is written in the form

$$\exp(-itH_z)=[\exp(-itH_z/M)]^M \equiv [U(t/M)]^M \quad . \tag{A1}$$

where a short-time propagator $U(t/M)$ is introduced, defined in eq. (A2), and where the number M is taken large enough so as to make the error term in (A2) small. We have for $U(\tau)$,

$$U(\tau) = \exp(-i\tau H_{el}/2)\exp(-i\tau K_z)\exp(i\tau H_{el}/2)+ 0(\tau^3) \quad , \tag{A2}$$

τ denoting t/M. Here, K_z denotes the nuclear kinetic energy operator, ($= -\frac{1}{2}\partial^2/\partial z^2$ in the z-representation). In the remainder of this Appendix we give the method for the three-coordinate case, where the evolution is discussed on the (2, 3) surfaces. For the one-coordinate case, the evolution was treated on the (1, 2, 3) surfaces, and the sums in (A3)-(A8) are then over $i = 1, 2, 3$.

H_{el} is the electronic Hamiltonian for motion on the (2, 3) pair of curves:

$$H_{el} = \sum_{i,j=2}^{3} |\psi_i\rangle\langle\psi_i|H_{el}|\psi_j\rangle\langle\psi_j| = \sum_{i=2}^{3} |a_i\rangle\langle a_i|H_{el}|a_i\rangle\langle a_i| \tag{A3}$$

where $|\psi_i\rangle$ is the ith diabatic electronic state and $|a_i\rangle$ refers to the ith adiabatic electronic state (cf eq. (A12) below for $|a_2\rangle$).

We define $|z_m\rangle$ as the eigenstate of the nuclear position operator z defined on a grid $\{z_m\}_{m=1}^N$ and write the total z-wave function, a function of z and t, as

$$|\Psi(z,t)\rangle = \sum_{m=1}^{N} \sum_{i=2}^{3} |z_m\rangle|\Psi_i\rangle \Phi_i(z_m, t) \ , \tag{A4}$$

where N is the number of grid points, the sum over i is over the diabatic electronic states 2 and 3, and $\Phi_i(z_m, t)$ is the value of the nuclear wave function at (z_m, t) for the ith electronic state. The total wave function at time $t+\tau$ is given by $|\Psi(z, t+\tau)\rangle = U(\tau)|\Psi(z, t)\rangle$. The long-time propagation is then achieved by successive applications of the short-time propagator (A2).

In order to calculate the $U(\tau)$ in eq. (A2), the $\exp(-i\tau H_{el}/2)$ in eq. (A2) is computed in a representation in which H_{el} is diagonalized with respect to the nuclear and electronic states. In particular, an adiabatic description is used for the electronic states and a coordinate description for the nuclear motion:

$$H_{el} = \sum_{i=2}^{3} \sum_{m=1}^{N} |a_i\rangle|z_m\rangle H_{ii} \langle z_m|\langle a_i| \ . \tag{A5}$$

For diagonalization of $\exp(-i\tau K_z)$, a representation in which K_z is diagonal is used, namely a diabatic description of the electronic states and a momentum representation for the nuclear motion:

$$K_z = \sum_{i=2}^{3} \sum_{m=1}^{N} |\Psi_i\rangle|z_m\rangle \tfrac{1}{2}P^2 \langle z_m|\langle \Psi_i| \ . \tag{A6}$$

We next introduce momentum eigenvectors for the nuclear motion $|k_n\rangle$, there being the set of points $\{k_n\}_{n=1}^{N}$ on a reciprocal space grid.[3b] Using the completeness $\sum_{n=1}^{N} |k_n\rangle\langle k_n| = 1$ and $\sum_{m=1}^{N} |z_m\rangle\langle z_m| = 1$ we have

$$K_z = \sum_{i=2}^{3} \sum_{l=1}^{N} \sum_{m=1}^{N} |\Psi_i\rangle|z_l\rangle \left\{ \sum_{n=1}^{N} \langle z_l | k_n \rangle \frac{k_n^2}{2} \langle k_n | z_m \rangle \right\} \langle z_m | \langle \Psi_i | \ . \qquad \text{(A7)}$$

Here $\langle z_l | k_n \rangle$ and $\langle k_n | z_m \rangle$ denote plane waves. Therefore, expressions of the form $\sum_{j=1}^{N} \langle k_n | z_j \rangle f(z_j)$ represent a Fourier Transform of $f(z)$, which will be denoted as $F[f]$.

By using Eqs. (A2) to (A7) we obtain

$$\Phi_i(z_m, t+\tau) = \sum_{j=2}^{3} \sum_{p=2}^{3} T_{ij} \exp(-i\tau\varepsilon_j/2)\, T^{\dagger}_{jp} F^{-1} \{ \exp(-i\tau k^2/2)$$

$$\sum_{r=2}^{3} \sum_{k=2}^{3} F[T_{pr} \exp(-i\tau\varepsilon_r/2)\, T^{\dagger}_{rk}\, \Phi_k(z_m, t)] \} \qquad \text{(A8)}$$

Here, the matrix element, T_{ij} denotes $\langle \Psi_i | a_j \rangle$.

To implement the method, the reaction coordinate z is first discretized, using a grid of N points and length L, with Δz ($=L/N$) being smaller than the length scale over which the nuclear wavefunctions Φ_k change significantly. At each point of the grid the initial wave functions Φ_k are transformed into adiabatic wave functions $T^{\dagger}_{rk}\Phi_k$, then operated on with the diagonal operator $\exp(-i\Lambda_{el}\tau/2)$, diagonal in this representation, and then transformed back into the diabatic representation, as in eq. (A8). This step couples the diabatic electronic states. Next, each diabatic component Φ_p is Fourier-transformed into the k-momentum representation, operated on by $\exp(iK_z\tau)$ and changed back into the z-coordinate representation using an inverse Fourier transform (cf. eq. (A8)). These operations couple the amplitudes $\{\Phi_p(z_m)\}$ at different points in the grid. To perform the Fourier transforms involved at this stage, an efficient fast Fourier transform algorithm was used. [4]

The times involved in the computation were long enough to allow the wave function ϕ to reach the edge of the grid. When this happens the piece of the wave function reaching the edge of the grid would normally reappear at the left hand side, since the fast Fourier transform method uses periodic boundary conditions. Such a reappearance, if allowed to occur, would distort the calculated values of the rate constant. To avoid this spurious consequence an absorbing boundary condition was, in effect, used, namely by using a complex-valued potential which removes the wavefunction before it reached the grid edge,[2] namely

$$H_{jj}^{(a)} = H_{jj} - iV_{abs}(z) \ , \tag{A9}$$

where H_{jj} are the diagonal elements of the potential matrix H_{el} and $V_{abs}(z)$ causes the absorption.

$$V_{abs}(z) = \exp[\gamma(z - z_L)] \tag{A10}$$

Here, z_L is a point close to the right hand edge of the grid and γ is a parameter that controls how rapidly ψ_j will decay to zero near that zone. The imaginary part of the potential namely , $-iV_{abs}(z)$, was chosen such that it tended to zero everywhere except near the edge of the grid.

We give below some further details on the calculations mentioned in the text:

When a purely adiabatic description is used for motion on the (2, 3) pair of surfaces, to compare with the previous calculations based on the H_z in eq. (4.4) of Part I,

$$H_z = \sum_{i=2}^{3} \sum_{j=2}^{3} |\psi_i\rangle(-\tfrac{1}{2}\frac{\partial^2}{\partial z^2}\delta_{ij} + H_{ij}(z))\langle\psi_j| \ . \tag{A11}$$

an adiabatic expression H_z^{ad} was used instead of this H_z

$$H_z^{ad} \equiv |a_2\rangle \left[-\frac{1}{2}\frac{\partial^2}{\partial z^2} + E_-(z) \right] \langle a_2| \quad , \qquad \text{(adiabatic)} \tag{A12}$$

where $|a_2\rangle$ is the adiabatic electronic state function for the lowest electronic adiabatic eigenvalue $E_-(z)$. In this second instance the z-adiabatic electronic-vibrational state function, $\Phi_2^{ad}(z, t)\,|a_2\rangle$, where $\Phi_2^{ad}(z, t)$ is the nuclear part and $|a_2\rangle$ the electronic part, is next transformed into its diabatic components.[3b] The z-nuclear wavefunction $\Phi_2(z, t)$ for electronic state 2, is then given by

$$\Phi_2(z, t) = \sum_{j=2}^{3} T_{2j}(z)\,\Phi_j^{ad}(z, t) = T_{22}(z)\,\Phi_2^{ad}(z, t)\,, \tag{A13}$$

since only one adiabatic electronic state $|a_2\rangle$ is considered. Here, T_{ij} is an element of the matrix T mentioned above, which transforms from the adiabatic to the diabatic representation, $T_{ij}(z) = \langle \psi_i | a_j(z) \rangle$; $|\psi_i\rangle$ and $|a_j(z)\rangle$ are the ith electronic diabatic and the jth adiabatic electronic state at the cited value of z, respectively ($i = 2, 3$; $j = 2, 3$). The $|a_j(z)\rangle$ and hence the $T_{ij}(z)$, depend parametrically on z. The transformation matrix T satisfies the relation $\Lambda_z = T^{\dagger} H T$, where H is a matrix with elements given by the $H_{ij}(z)$ terms in eq. (A11) and Λ_z is the diagonal matrix whose elements are the adiabatic eigenvalues $E_+(z)$ and $E_-(z)$. The columns of the T are the eigenvectors of this H_z.

Appendix B. Approximations used for k_r

(i) Airy function calculation for $\phi_{m'}(z)$

The pair of potentials $H_{22}(z)$, $H_{33}(z)$ in eq. (2.4), given by eq. (2.2) with the modification noted in Section II(*i*) for $x > b$, and with a coupling element H_{23}, are used to calculate $E_{-}(z)$ and, thereby, the $\phi_A(z)$'s. The reactant's vibrational wave function $\phi_m(z)$ for electronic state 1 is a normalized bound state wavefunction, while the wavefunction $\phi_{m'}$, given by the ϕ_A, is normalized to a Dirac delta function in energy differences,[10] the latter in units of $\hbar\omega$.

This approximation for ϕ_A employs a uniform semiclassical function based on an Airy function, which when normalized to a Dirac delta function is given by[11]

$$\phi_A(z) = 2^{\frac{1}{2}}[\xi(z)]^{\frac{1}{4}}[k(z)]^{-\frac{1}{2}} Ai(-\xi(z)) \quad , \tag{B1}$$

where

$$k^2(z) = 2(E - E_{-}) \; , \; \xi(z) = \left(\frac{3}{2}\int_{z_o}^{z} k(z)dz\right)^{\frac{2}{3}} \quad , \tag{B2}$$

$E - E_{-}$ being in units of $\hbar\omega$, $E_{-}(z)$ is given by eq. (2.4), modified for $z \geq b$ as noted earlier, and

$$Ai(-\xi) = \frac{1}{2\pi}\int_{-\infty}^{\infty} exp\left(\frac{is^3}{3} - is\xi\right)ds \quad , \tag{B3}$$

The z_o in eq. (B1) is the classical turning point for nuclear motion on the curve $E_{-}(z)$ at the energy E.

(ii) Harmonic $\phi_{m'}(z)$ calculation

This calculation of k_r is the standard one, and involves choosing $\phi_{m'}(z)$ to be a vibrational eigenstate of the harmonic oscillator Hamiltonian eq. (3.7) of Part I with $H_{22}(z)$ given by the present eq. (2.2). The resulting k_r in Tables I and II is denoted by

k_{HO}. For a one-dimensional problem the density of harmonic oscillator vibrational states in electronic state ψ_2 is $(\hbar\omega)^{-1}$, and so the sum over the final vibrational states approaches $(\hbar\omega)^{-1}$ (and hence unity in the present dimensionless quantities) times the value of the overlap integral squared, interpolated from the discrete states $\phi_{m'}$ to an energy where $E_{m'}=E_m$. Each of the functions ϕ_m and $\phi_{m'}$ is now a (normalized) harmonic oscillator wavefunction because of the harmonic potentials $H_{11}(z)$ and $H_{22}(z)$ used in eq. (2.2).

(*iii*) *Semiclassical Results*

A stationary phase semiclassical approximation to two of the above solutions – the adiabatic one in section (*i*) and the harmonic-harmonic in section (*ii*) is readily obtained: WKB solutions are introduced for the wavefunctions appearing in the integral $\langle\phi_m|\phi_{m'}\rangle$, in eq. (2.3), which is then given by:[11]

$$\langle\phi_m|\phi_{m'}\rangle = F(z_c)\sin[\Theta(z_c)+\frac{\pi}{4}] \tag{B4}$$

where

$$\Theta(z)=\int_{z_1}^{z} k_m(r)dr - \int_{z_{m'}}^{z} k_{m'}(r)dr \ . \tag{B5}$$

and

$$F(z_c)=\frac{1}{\pi k_m(z_c)}\left(\frac{2\pi}{|\Theta''(z_c)|}\right)^{\frac{1}{2}} = \left(\frac{2}{\pi k_m(z_c)|s_1-s_{m'}|}\right)^{\frac{1}{2}} \tag{B6}$$

where the fact that $k_m(z_i)=k_m'(z_c)$ was used, and where $s_1-s_{m'}$ denotes the difference in slopes of the potential energy curves $H_{11}(z)$ and either $H_{22}(z)$ (for $k_r=k_{HO}^{sc}$) or $E_{-}(z)$ (for $k_r=k_A^{sc}$) at the crossing point $z=z_c$. Normally, the constant $F(z_c)$ would differ by a factor of $(\hbar\omega)^{\frac{1}{2}}$, depending on whether a wavefunction $\phi_{m'}$ was normalized to a delta function of the energy or whether as in a bound state, to a delta function of the

quantum numbers.[10] In the present case, however, where we have employed dimensionless energies, the two normalizations are identical.[12]

In eq. (B5) k_m is $[2(E-H_{11}(z))]^{\frac{1}{2}}$ and $k_{m'}$ is $[2(E-H_{22}(z))]^{\frac{1}{2}}$ or $[2(E-E_-)]^{\frac{1}{2}}$, according as $H_{22}(z)$ or E_- is the potential used. z_c is the crossing point between the curves $H_{11}(z)$ and $H_{22}(z)$ [or $E_-(z)$] and z_1, $z_{m'}$ are the left hand classical turning points for nuclear motion in the potential energy curves $H_{11}(z)$ and $H_{22}(z)$ [or $E_-(z)$], respectively.

When the system was in the $m = 0$ state, the energy of that initial vibrational state was typically somewhat close to the potential energy at the crossing point x_c. For each such calculation in the semiclasssical case, a uniform approximation version of eq. (B4) was used, namely[13]

$$\langle \Phi_m | \Phi_j \rangle = (|F(z_c)|\pi)^{\frac{1}{2}} \zeta^{\frac{1}{2}} \mathrm{Ai}(-\zeta) \ , \tag{B7}$$

where $F(z_c)$ is given by (B6) and where ζ is positive and equals $(3/2|\Theta(z_c)|^{\frac{1}{2}}$.

References

1. Marcus, R. A.; Almeida, R. *J. Phys. Chem.*, submitted.
2. Almeida, R.; Metiu, H., unpublished.
3. (a) E. g., Feit, M. D.; Fleck, Jr., J. A.; Steiger, A. *J. Comp. Phys.*, **1982**, *47*, 412. Kosloff, D.; Kosloff, R. *J. Comp. Phys.*, **1983** *52*, 35,(b) Alvarellos, J.; Metiu, H. *J. Chem. Phys.* **1988**, *88*, 4957. Almeida, R. *Ph.D. Thesis*, University of California, Santa Barbara, 1987, Ch. 5.
4. We used the FFT routines available in the IMSL Library.
5. E. g., Merzbacher, E. *Quantum Mechanics*; Wiley: New York, 1970.
6. E. g., Marcus, R. A.; Sutin, N. *Biochim. Biophys. Acta* **1985**, *811*, 265.
7. For example, when the 2→3 transition is in the "inverted" region, discussed in ref. 6, ($-\Delta E_{23} > \lambda_{23}$), a large value of the H_{23} matrix element makes the 2→3 process highly nonadiabatic and so makes w_{23} small. There then tends to be an oscillatory behavior between the D*BA and the D^+B^-A electronic configurations, instead of a largely first-order decay of D*BA. (Cf. Fig. 3.) In all of the results in Table IV either $-\Delta E_{23} < \lambda_{23}$ or $-\Delta E_{23} \simeq \lambda_{23}$.
8. Martin, J.-L.; Breton, J.; Lambry, J.-C.; Fleming, G.R., in *The Photosynthetic Reaction Center - Structure and Dynamics. NATO ASI Series A: Life Sciences* **1988**, *149*, 195. Room temperature results were obtained in references cited therein, and for *Rb. capsulatus* were obtained by Kirmaier, C.; Holten, D. *Isr. J. Chem.* **1988**, *152*, 79.
9. Holzapfel, W.; Finkele, U.; Kaiser, W.; Oesterhelt, B.; Scheer, H.; Stilz, H.U.; Zinth, W. *Chem. Phys. Lett.* **1989**, *160*, 1.
10. Child, M. in *Semiclassical Methods in Molecular Scattering and Spectroscopy*. NATO ASI Ser., Ser. C: Mathematical and Physical Sciences **1979**, *53*, 127.
11. Child, M. S. *Mol. Phys.* **1975**, *29*, 1421, Ref. 10, p. 131.

12. E. g., for a bound state one uses a normalization to $\delta_{m,m'}$, or, when the levels are so closely spaced that sums can be replaced by integrals, to $\delta(m-m')$. But $\delta(m-m')=\hbar\omega\,\delta(E_m-E_{m'})$, leading to a normalization of the $\psi_{m'}$ for an unbound state which differs from that of the bound state $\psi_{m'}$ by a factor of $(\hbar\omega)^{\frac{1}{2}}$ or, in the present case of dimensionless units, which is identical, $\delta(m-m')=\delta(E_m-E_{m'})$ when the E's are in units of $\hbar\omega$.

13. Ref. 10, cf. eqs. 20 and 27a with the present (B4) and (B7).

Legend to Figures

Fig. 1 Typical semilog plot of logarithm of survival probability $D^*(t)$ vs. t for the one-coordinate calculation. $\Delta E_{12} = -1.5$, $\Delta E_{13} = -15$, $m = 0$, and remaining parameters are given in Footnote a of Table I; a and b in eq. (2.2) are both positive.

Fig. 2 Fit of $B^-(t)$ in the 1-D calculation to an effective two-step incoherent formalism, using only $k_2 = 24$ ps^{-1} as a single empirical parameter. For these results we have $\Delta E_{12} = -2.5$, $\Delta E_{13} = -15$, $m = 0$ and the remaining parameters are given in Footnote a of Table I; a and b in eq. (3.2) are both positive.

Fig. 3 Example of the time-evolution of $D^*(t)$ in a 1-D calculation for the case when ω_{23} is made quite small (see text), by having the 2→3 transition in the inverted region ($-\Delta E_{23} > \lambda_{23}$), and with a large value of H_{23}. In the case depicted, $-\Delta E_{23} = 19.5$, $\lambda_{23} = 3.08$, $-\Delta E_{12} = 1.5$, and $\lambda_{12} = 3.58$.

Fig. 4 Plot of B_{max}^- vs. $z_{23}^\ddagger - z_{12}^\ddagger$, given by (2.7), for $H_{23}/H_{12} = 6$, and several families of λ's used in Table IV: □, $\lambda_1 \sim \lambda_2$ (within a factor of 2); ●, $\lambda_2 = 0.1$; ×, $\lambda_2/\lambda_1 \sim 1.5$ to 1/6. Data taken from Table IV.

Fig. 5 Plot of B_{max}^- vs. $z_{23}^\ddagger - z_{12}^\ddagger$, given by (2.7), for $H_{23}/H_{12} = 10$, (data in Table IV).

Fig. 6 Plot of $B_{ad,max}^-$ vs. $z_{23}^\ddagger - z_{12}^\ddagger$, given by (2.7), for $H_{23}/H_{12} = 6$, (data in Table IV).

Fig. 7 Plot of $B_{ad,max}^-$ vs. $z_{23}^\ddagger - z_{12}^\ddagger$, given by (2.7), for $H_{23}/H_{12} = 10$, (data in Table IV).

Fig. 8 Fit of $B^-(t)$ in the 3-D calculation to an effective two-step incoherent formalism, using only a $k_2 = 22$ ps^{-1} as a single empirical prameter. These results correspond to the ninth row of Table IV, in the column of $B_{max}^{-(c)}$.

Fig. 9 Fit of $B^-(t)$ in the 3-D calculation to an effective two-step coherent formalism, using only a $k_2 = 12$ ps^{-1} as a single empirical parameter. These results correspond to the fourth row from the bottom in Table IV, in the column of $B_{max}^{-(c)}$.

Table I. First-order rate constants (ps^{-1}) for various initial vibrational states m (1-coordinate calculation).[a]

m	ΔE_{12}	k_1 [b]	k_A [c]	k_A^{sc} [d]	k_{HO} [e]	k_{HO}^{sc} [d]
0	−0.5	1.99	2.17	2.20	2.09	2.08
1		0.0063	0.011	0.011	0.022	0.026
2		0.55	0.56	0.57	0.84	0.87
3		0.80	0.91	0.91	1.04	1.06
4		0.78	0.83	0.82	0.73	0.71
0	−1.5	1.52	1.62	1.64	1.56	1.56
1		0.0094	0.0091	0.0089	0.062	0.064
2		0.61	0.67	0.70	0.83	0.85
3		0.59	0.63	0.62	0.52	0.51
4		0.092	0.095	0.090	0.15	0.14
0	−2.5	1.11	1.21	1.22	1.15	1.14
1		0.10	0.11	0.11	0.22	0.22
2		0.61	0.71	0.72	0.73	0.73
3		0.14	0.15	0.19	0.11	0.10
4		0.069	0.053	0.050	0.12	0.13
0	−3.5	0.92	1.07	1.06	1.01	0.99
1		0.12	0.13	0.13	0.23	0.23
2		0.54	0.63	0.64	0.62	0.62
3		0.067	0.087	0.085	0.032	0.029
4		0.16	0.13	0.14	0.22	0.23

a For a $-\Delta E_{12}$ of 0.5, 1.5, 2.5 and 3.5, in dimensionless units, the values of λ_{12} were (to three figures) 1.62, 2.82, 4.30, and 5.52, respectively, λ_{13} was (to three figures) 21.9, 21.4, 21.0 and 20.9, respectively, and $-\Delta E_{13} = 15$, $H_{12} = 0.25$, $H_{23} = 2.5$. The height ΔV_1 of the crossing point of H_{11} and H_{22} was between 0.15 and 0.2, namely (as calculated from eq. (2.5)) 0.194, 0.155, 0.188 and 0.165, respectively. The a and b in eq. (2.2) were chosen to be of the same sign.

b Calculated using the FFT method.

c Calculated using only the cited m term in eq. (2.3) and using eq. (B1) for the $\phi_m(z)$ in eq. (2.3) and integrating in $\langle\phi_m|\phi_m\rangle$ numerically to obtain this matrix element.

d Calculated semiclassically using only the cited m term in eq. (2.3) and using eqs. (B4)-(B6). For $m = 0$ eq. (B7) was always used.

e Calculated from eq. (3.13) of Part I.

Table II. First-order rate constants (ps^{-1}) for various initial vibrational states m (1-coordinate calculation).[a]

m	ΔE_{12}	$\Delta \bar{V}_1$	k_1 [b]	k_A [c]	k_A^{sc} [d]	k_{HO} [e]	k_{HO}^{sc} [d]
0	0	0.76	0.44	0.54	0.52	0.44	0.41
1			1.32	1.35	1.33	1.47	1.56
2			0.21	0.16	0.17	0.080	0.081
3			R	0.14	0.13	0.23	0.24
4			0.89	0.68	0.67	0.69	0.69
0	−0.5	0.54	0.76	0.78	0.77	0.70	0.67
1			0.80	0.93	0.94	1.09	1.12
2			0.50	0.55	0.57	0.46	0.47
3			0.0091	0.0097	0.0089	0.00014	0.00042
4			0.39	0.45	0.45	0.54	0.54
0	−1.5	0.20	1.23	1.46	1.45	1.42	1.40
1			0.094	0.095	0.093	0.16	0.16
2			0.82	0.83	0.83	0.87	0.88
3			0.33	0.39	0.59	0.35	0.53
4			0.053	0.064	0.061	0.031	0.028
0	−2.5	0.025	1.42	1.74	1.86	1.72	1.89
1			0.17	0.16	0.15	0.11	0.11
2			0.09	0.11	0.12	0.30	0.31
3			0.61	0.61	0.63	0.71	0.72
4			0.28	0.59	0.59	0.41	0.40

a We have set $-\Delta E_{13} = 15$, $\lambda_{12} = 3.03$ (to three figures), $\lambda_{23} = 21$, $H_{12} = 0.25$, $H_{23} = 1.75$ and $\hbar\omega = 100\ cm^{-1}$. The a and b in eq. (2.2) were chosen to be of the same sign.

b Calculated using the FFT method. The R in the fourth entry of this column denotes a resonance-like behavior.

c, d, e See corresponding footnotes in Table I.

Table III. k_2's fitted to $B^-(t)$ Curves, One-Coordinate Calculations [a]

m	ΔE_{12}	k_1 (ps^{-1})	k_2 (ps^{-1})	$z_{23}^{\ddagger} - z_{12}^{\ddagger}$
0	−0.5	1.99	29	0.41
0	−1.5	1.23	28	0.67
0	−2.5	1.42	24	0.57
0	−3.5	0.92	25	0.63

[a] The molecular parameters (λ's, etc.) are given in Footnote *a* of Table I.

Table IV. Maximum Population P_2 for Several Potential Energy Surfaces. [a]

$-\Delta E_{12}$	$-\Delta E_{13}$	λ_1	λ_2	λ_1	$B_{ad,max}$ [b] (%)	B_{max} [b] (%)	$z_{23}^{\ddagger} - z_{12}^{\ddagger}$ (x 0.1)	$B_{ad,max}$ [c] (%)	B_{max} [c] (%)
3.5	21	2.85	2.9	18.15	1.5	6.9	−2.0	1.3	6.0
2.5	21	2.4	2.4	18.6	1.4	5.8	−2.0	1.3	3.5
1.5	21	1.9	1.9	19.1	1.4	5.1	−2.0	1.3	3.0
3.5	19	5.65	0.1	15.35	1.6	4.8	−0.4	1.5	5.4
1.5	19	3.7	0.1	17.3	1.8	4.4	−0.4	1.8	4.1
2.5	21	2.4	2.4	20	2.4	6.5	0.4	2.2	3.7
1.5	21	1.9	1.9	21	2.6	5.9	1.1	2.5	2.95
3.5	21	2.85	2.9	21	3.1	7.6	1.1	2.4	3.8
3.5	17	5.65	0.1	15.35	2.9	6.4	3.2	2.5	3.4
1.5	17	3.7	0.1	17.3	3.1	5.85	3.0	3.0	3.45
1.5	15	3.7	0.1	15.3	3.4	6.1	3.2	3.2	3.4
1.5	15	3.7	0.1	16.3	4.2	6.3	4.8	4.1	4.0
3.5	15	5.65	0.1	15.35	5.0	7.05	6.8	4.3	4.6
2.5	15	4.7	0.1	16.3	5.0	7.15	6.5	4.6	4.8
1.5	15	3.7	0.1	17.3	5.1	7.2	6.4	4.8	4.95
2.5	15	4.0	0.8	17	5.85	9.9	6.8	5.3	5.4
3.5	15	5.0	0.75	16	6.0	9.4	7.1	5.3	5.6
2.5	15	3.5	1.3	17.5	7.9	14.4	7.1	5.6	5.9
2.5	15	4.0	1.75	17	9.0	15.0	7.3	6.2	6.6
3.5	15	3.0	1.8	18	9.6	16.4	7.2	6.05	6.6
3.5	13	5.65	0.1	15.35	7.8	12.2	10.4	6.5	6.6
1.5	13	3.7	0.1	17.3	8.1	13.7	9.8	7.1	7.3

[a] When $\Delta E_{12} = -1.5$ and $\Delta E_{12} = -3.5$ a $k_r = 0.92\ ps^{-1}$ was used, while when $\Delta E_{12} = -2.5\ ps^{-1}$ a $k_r = 0.93\ ps^{-1}$ was employed.

[b] $H_{23}/H_{12} = 6$

[c] $H_{23}/H_{12} = 10$

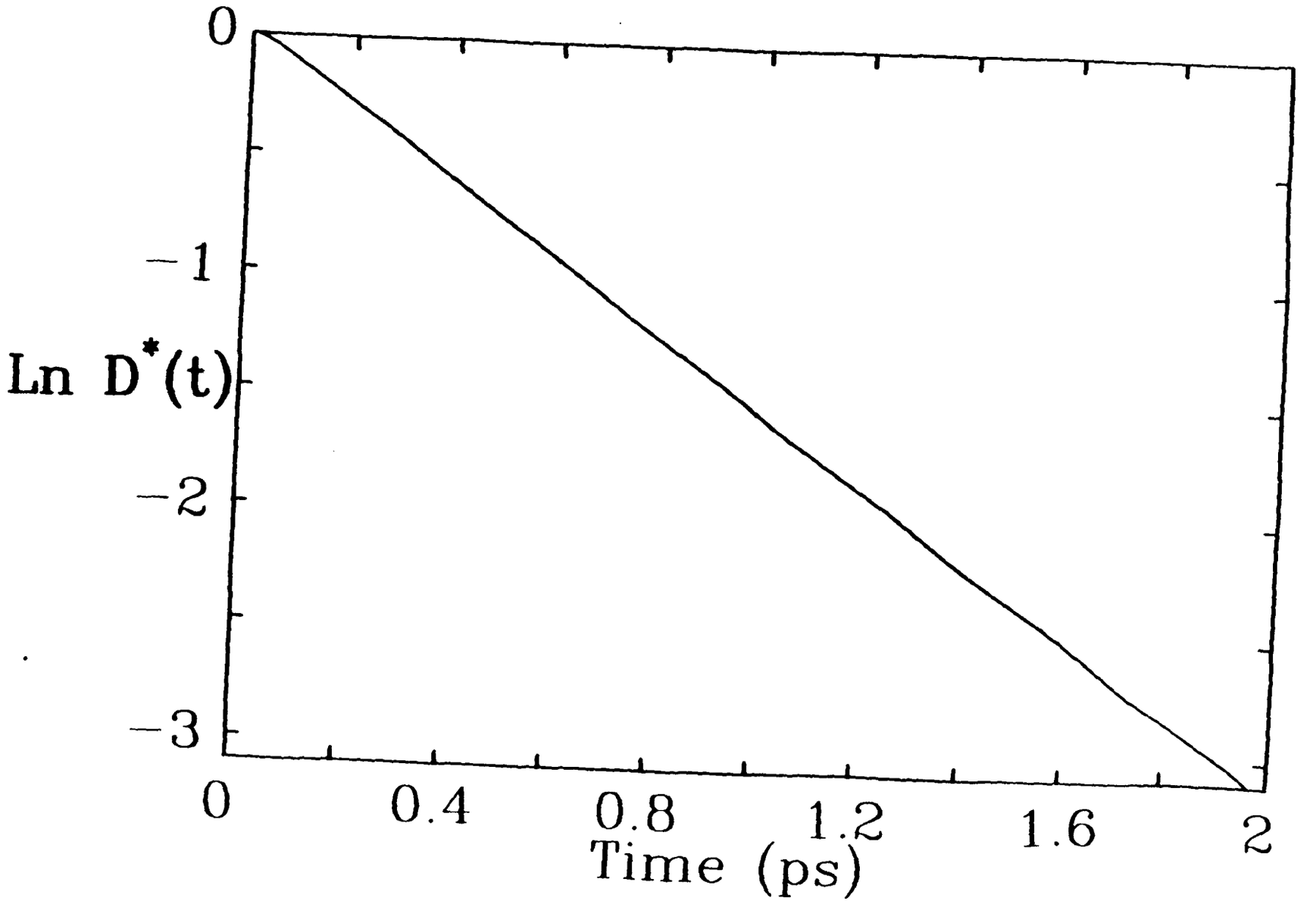
0
−1
−2
−3
Ln D*(t)
0
0.4
0.8
1.2
1.6
2
Time (ps)

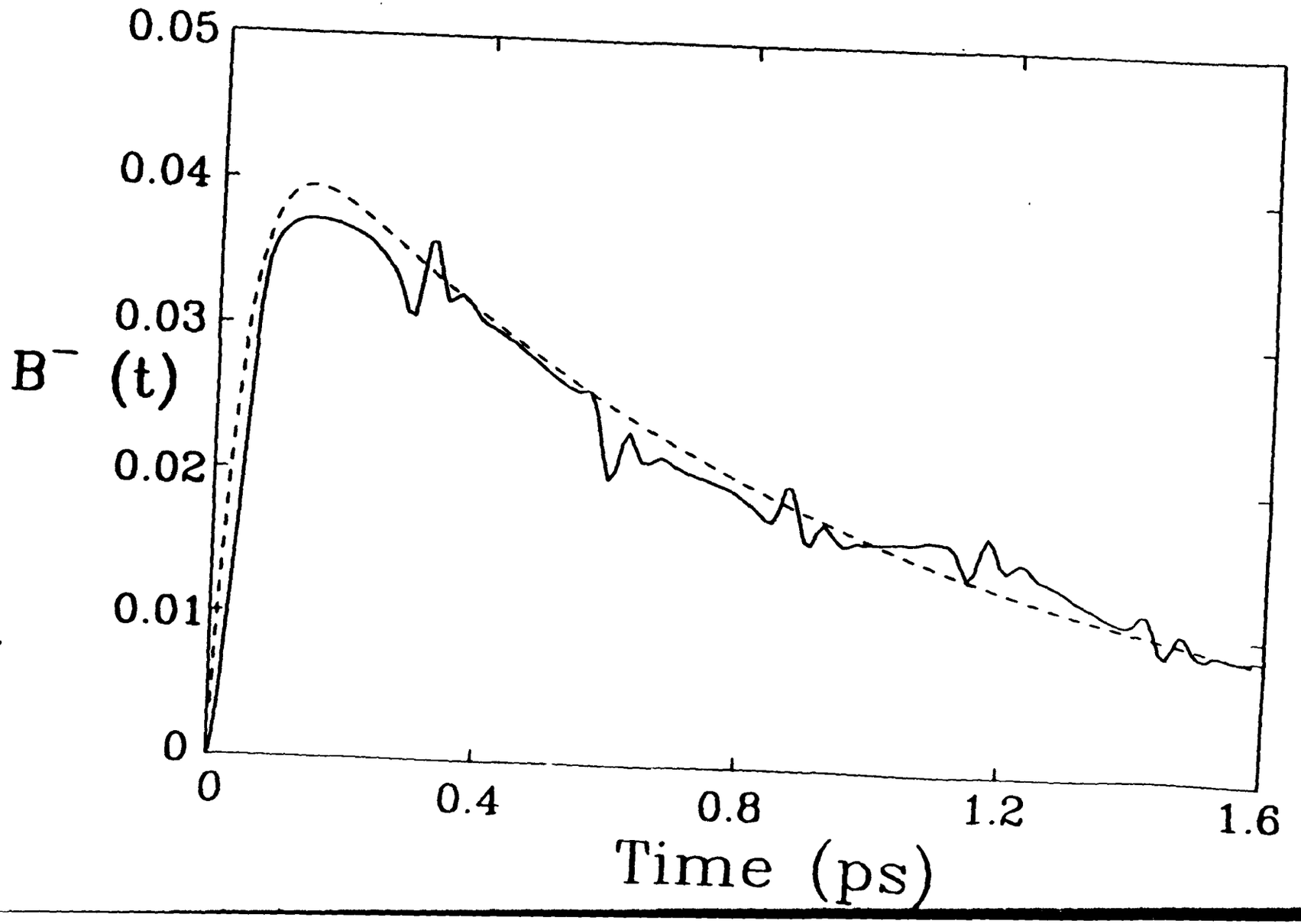
0.05
0.04
0.03
0.02
0.01
0
B⁻ (t)
0
0.4
0.8
1.2
1.6
Time (ps)

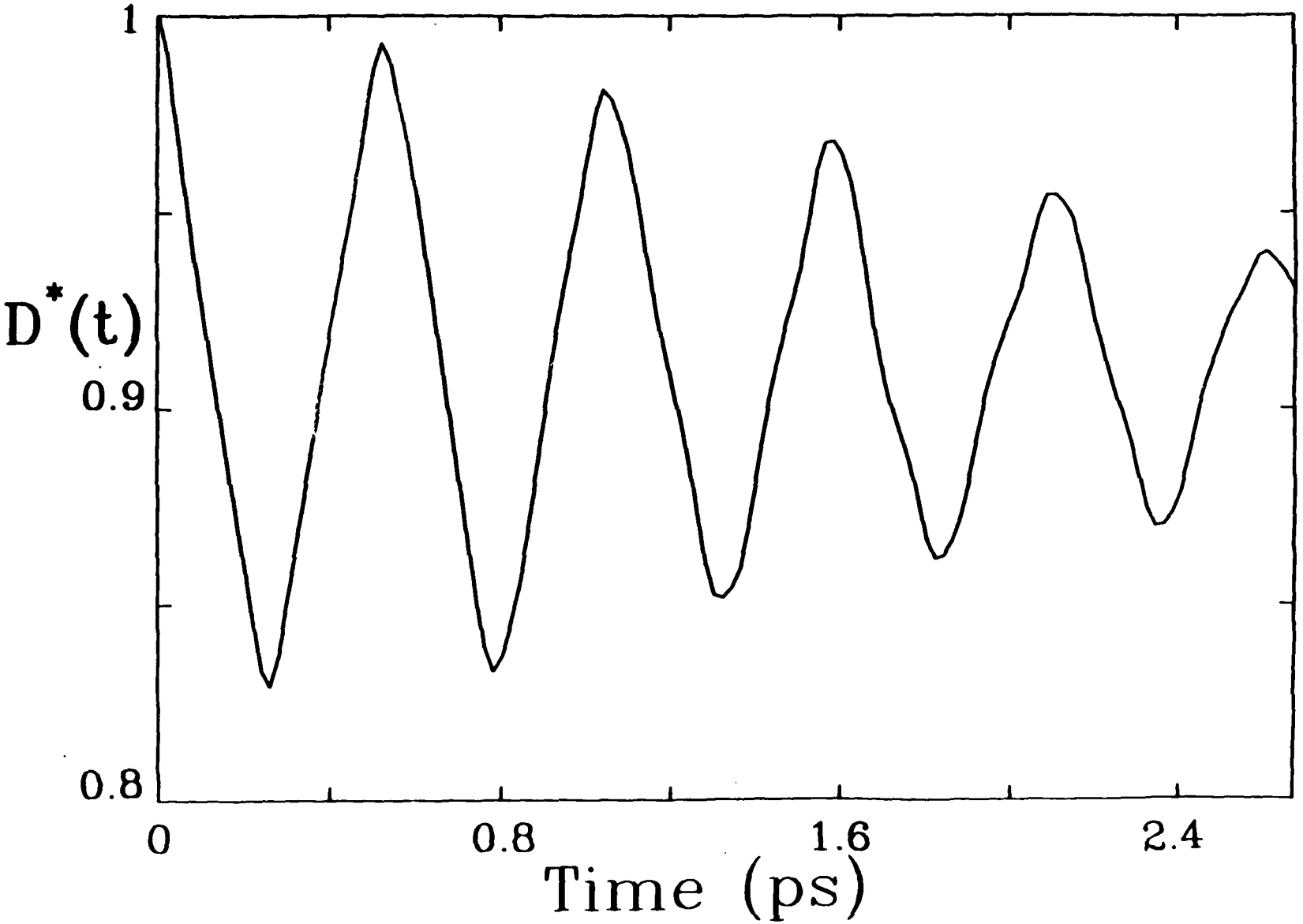
1
D*(t)
0.9
0.8
0
0.8
1.6
2.4
Time (ps)

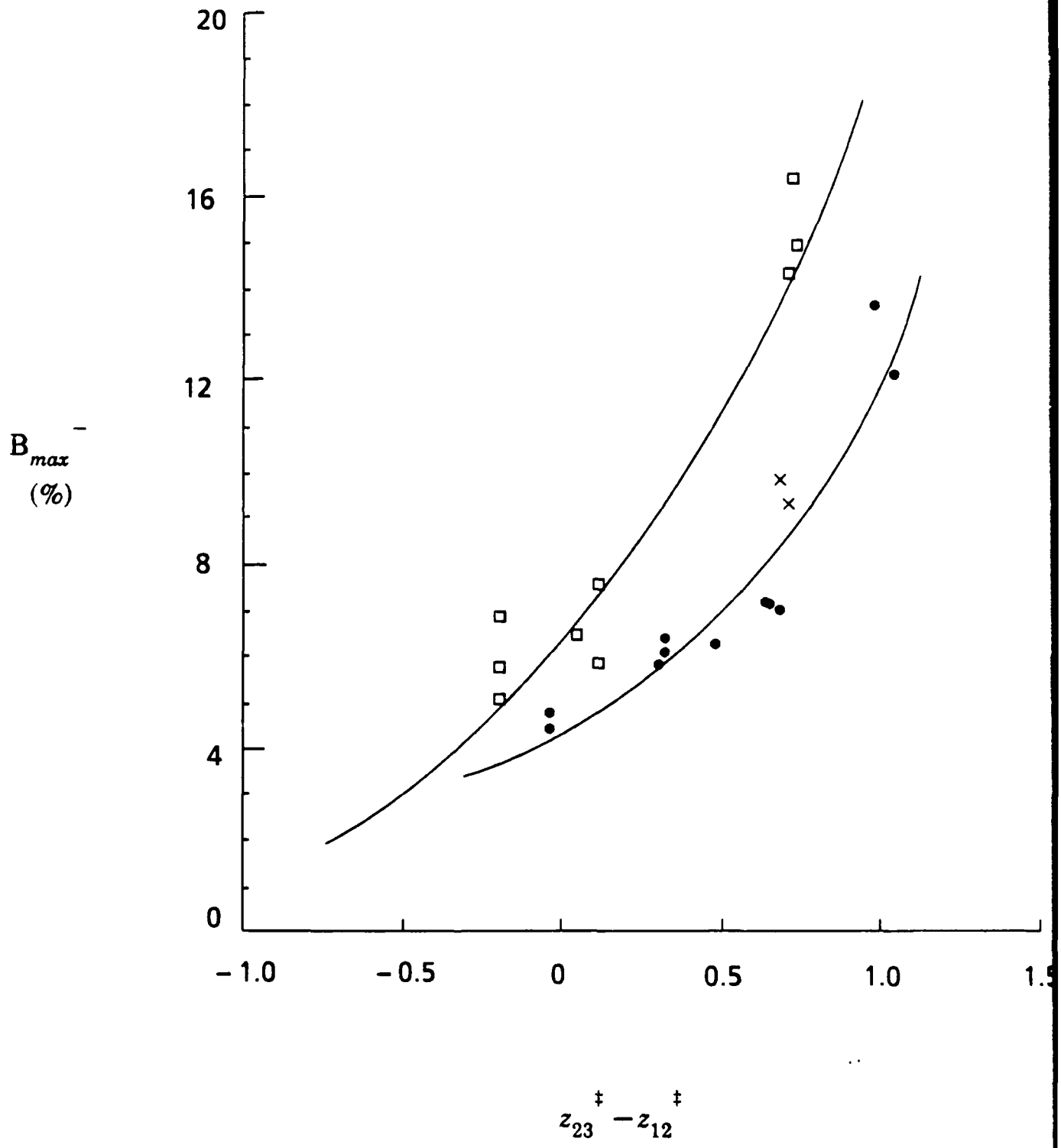

Fig. 4

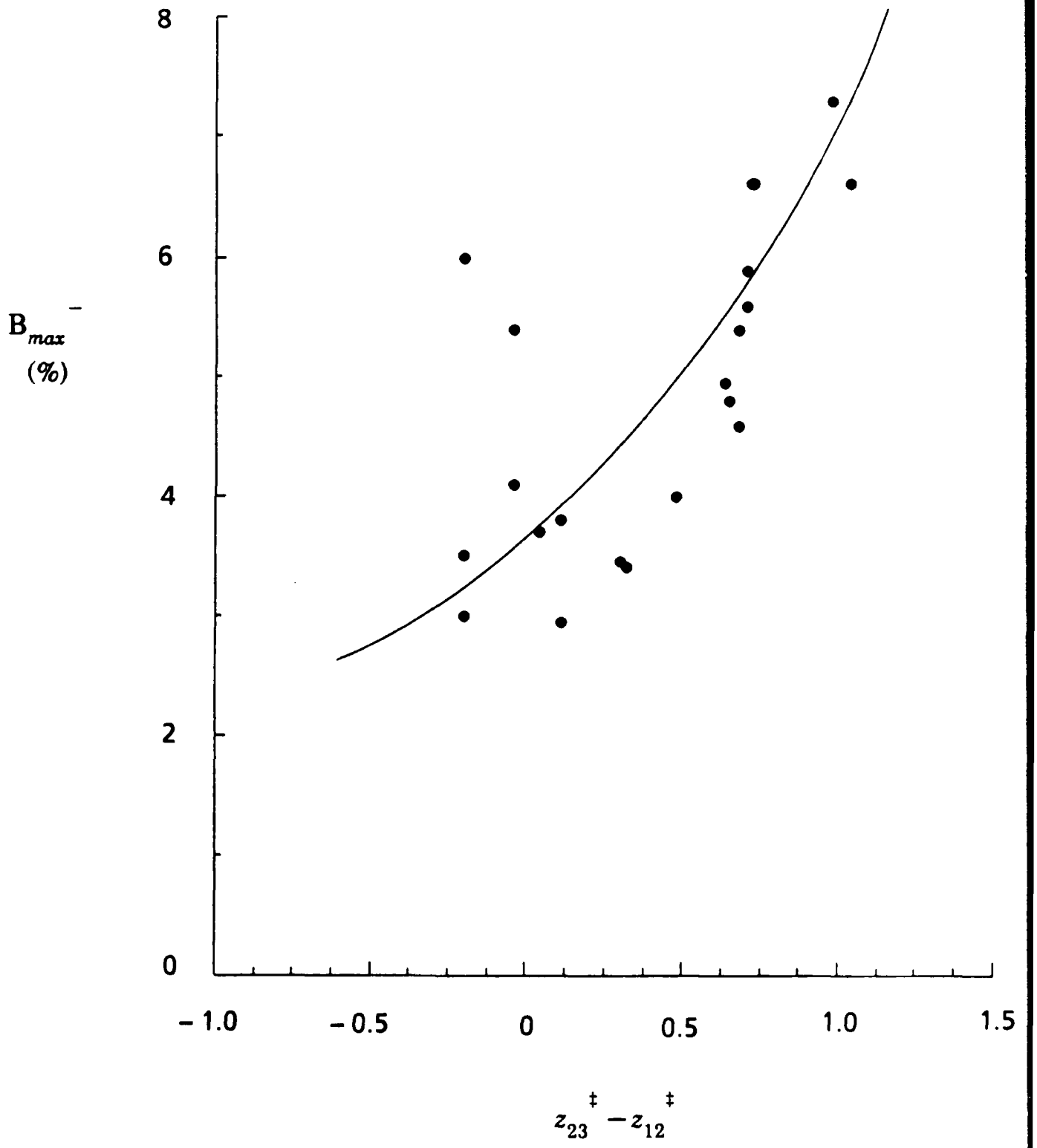

Fig. 5

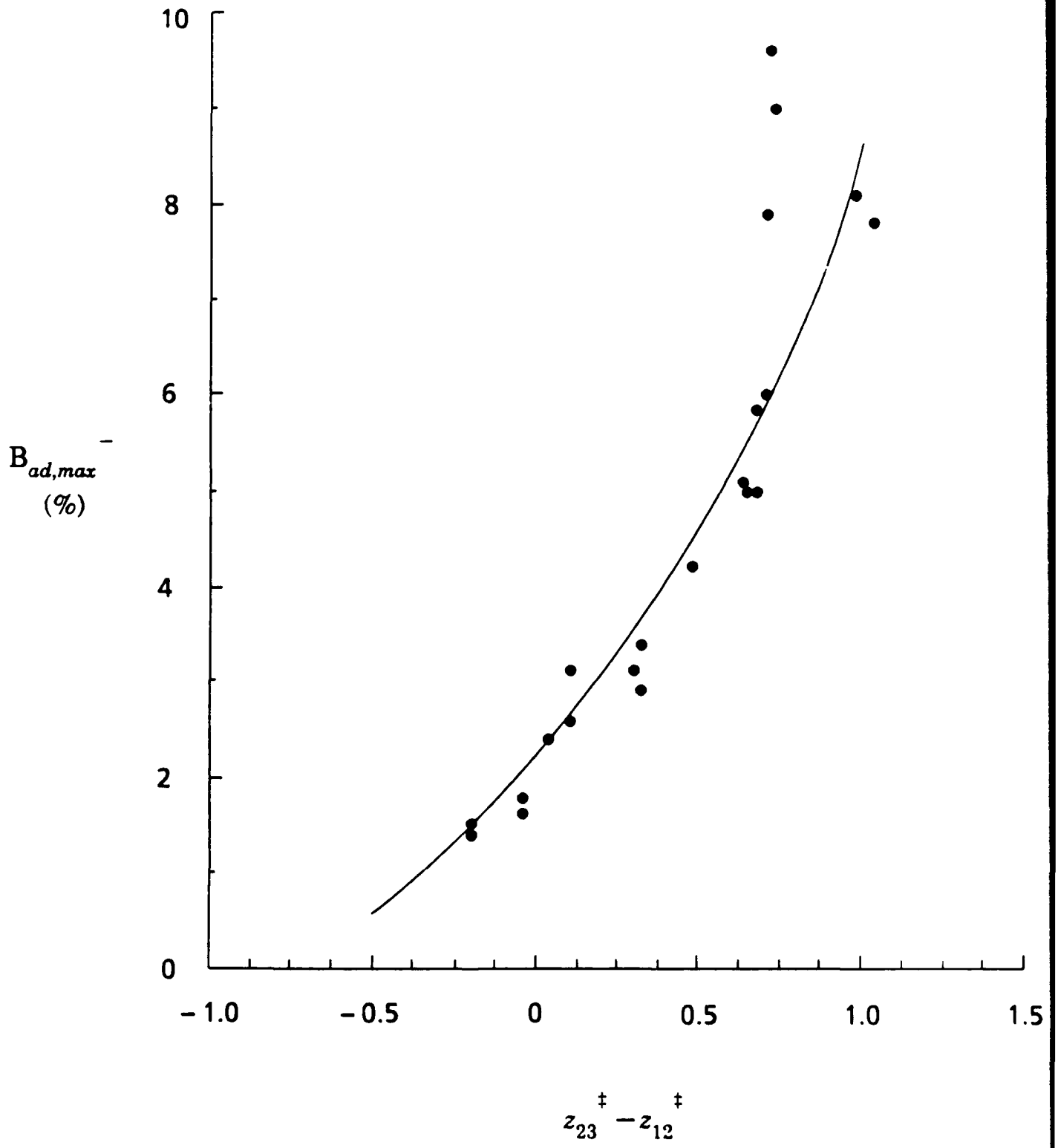

Fig. 6

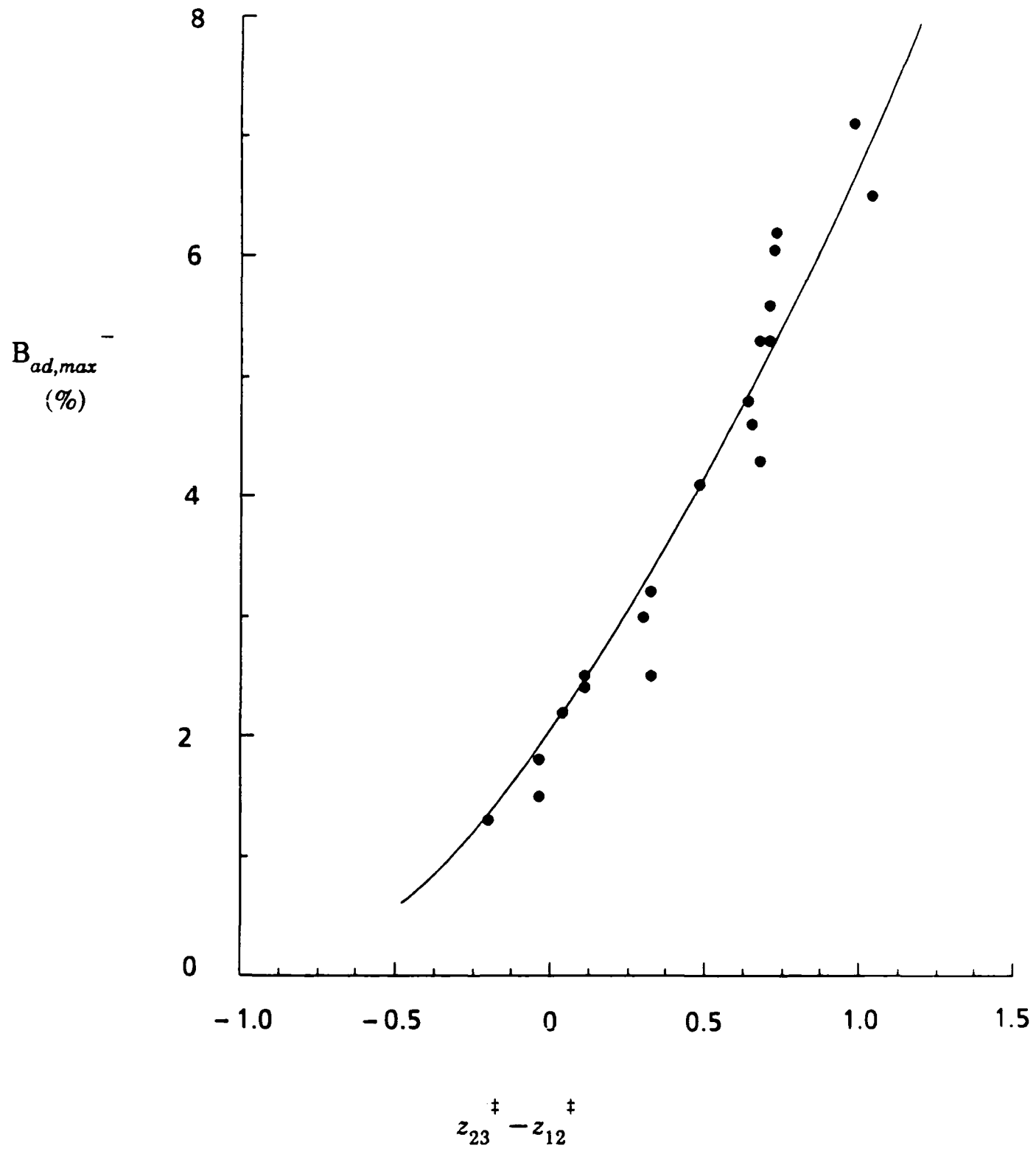

Fig. 7

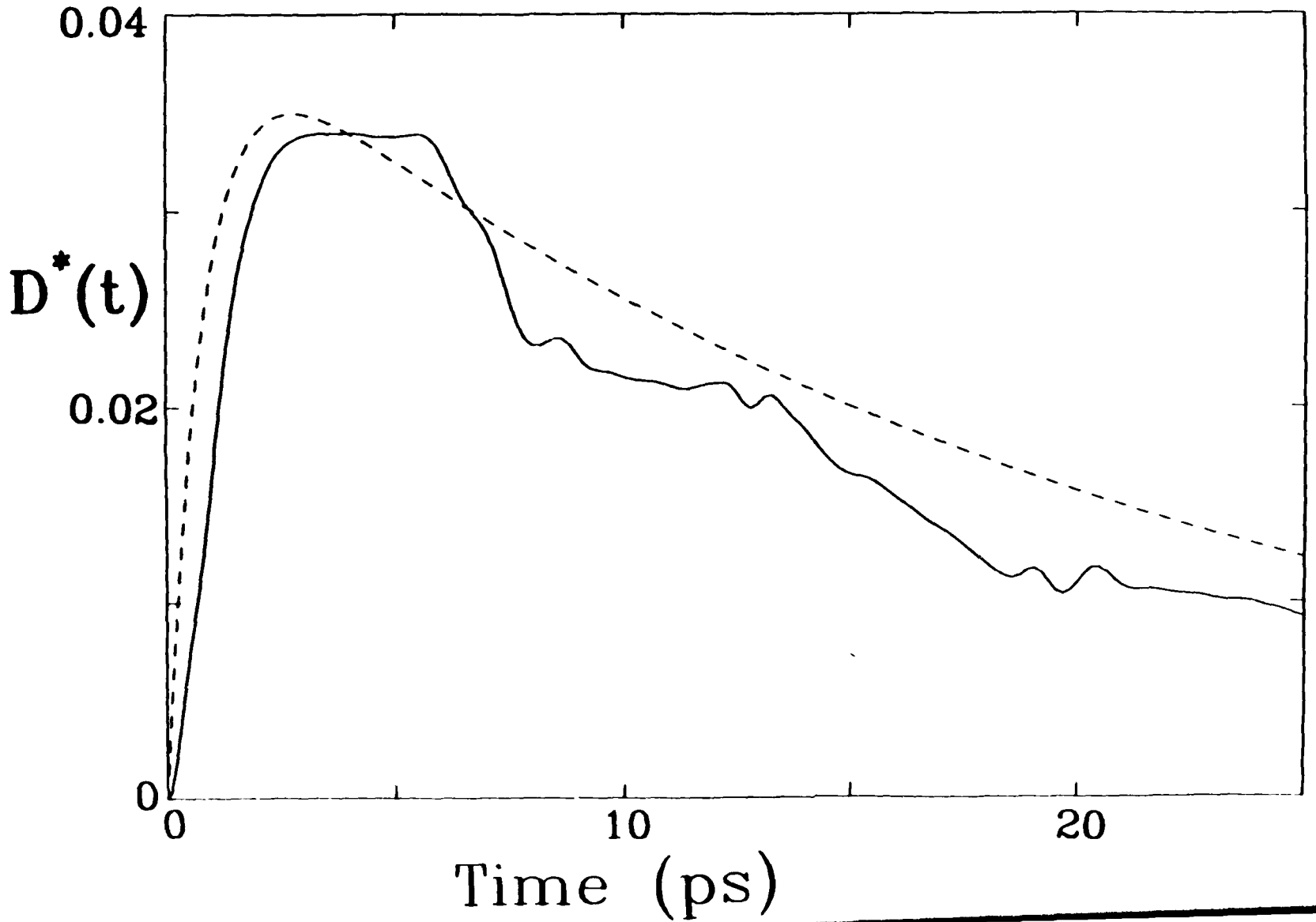
0.04
0.02
0
D*(t)
0
10
20
Time (ps)

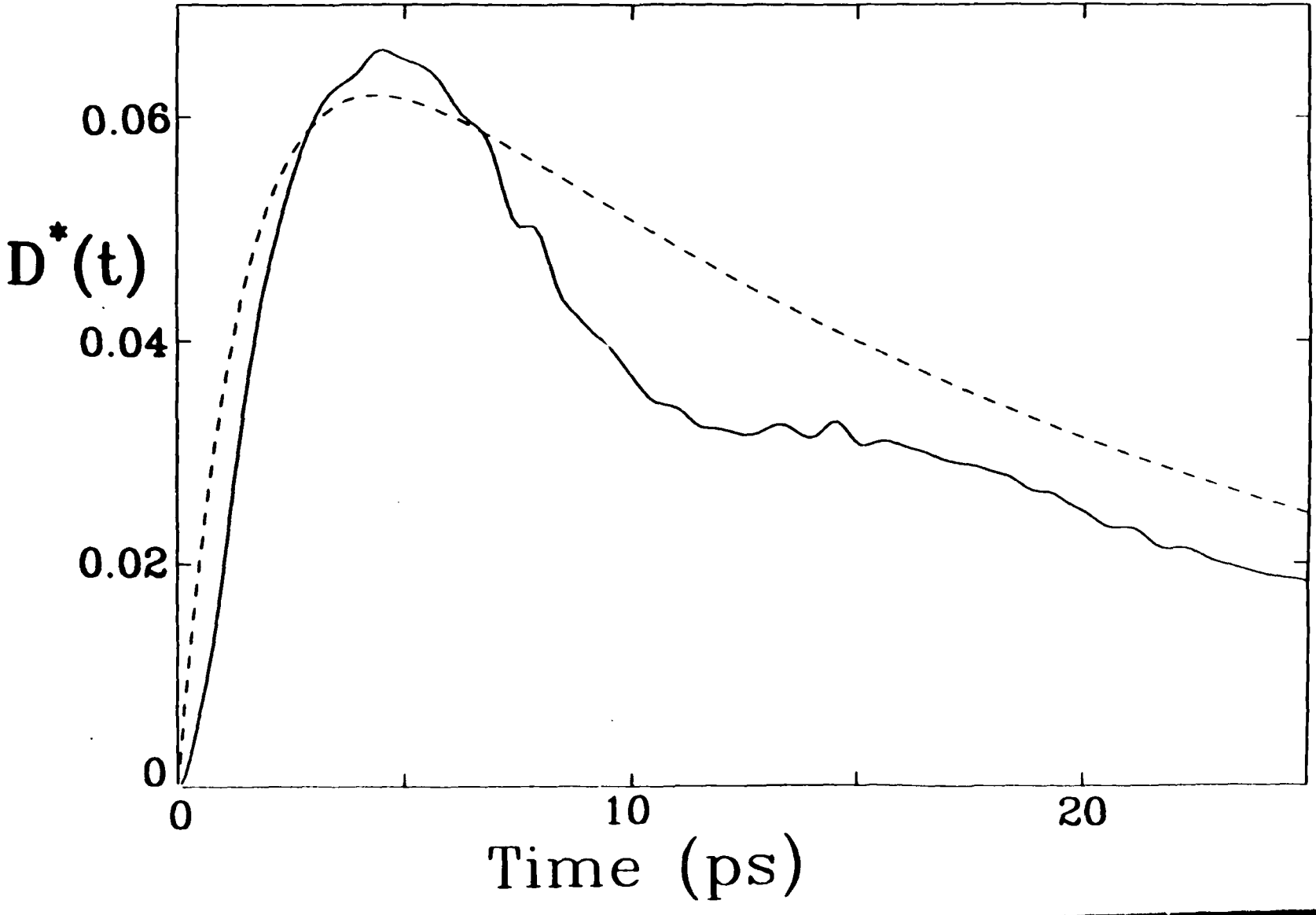
0.06
0.04
0.02
0
D*(t)
0
10
20
Time (ps)